Hierarchical Construction of Self-Standing Anodized Titania Nanotube Arrays and Nanoparticles for Efficient and Cost-Effective Front-Illuminated Dye-Sensitized Solar Cells

Qing Zheng,[†] Hosung Kang,[‡] Jongju Yun,[†] Jiyong Lee,[†] Jong Hyeok Park,[‡,§] and Seunghyun Baik[†,‡,⊥,*]

[†]Department of Energy Science, [‡]SKKU Advanced Institute of Nanotechnology (SAINT), [§]Department of Chemical Engineering, [⊥]School of Mechanical Engineering, Sungkyunkwan University, Suwon, Gyeonggi-do 440-746, Republic of Korea

ABSTRACT We report on the influence of hierarchical structures, constructed *via* layer-by-layer assembly of self-standing titania nanotube arrays and nanoparticles, upon charge recombination and photoelectric performance of front-illuminated dye-sensitized solar cells. Both nanotubes and nanoparticles were produced by anodization rather than additionally employing other methods, providing low cost and great simplicity. Electrochemical impedance spectroscopy under AM 1.5 illumination indicates the construction of hybrid morphology has superior recombination characteristics and a longer electron lifetime than nanoparticulate systems. This enhancement with the incorporation of anodized titania nanoparticles with 1D architectures is unprecedented for solar cells. Owing to the better light harvesting efficiency, extended electron lifetime and desirable electron extraction, the short-circuit photocurrent density of solar cell is 18.89 mA cm^{-2} with an overall power conversion efficiency of 8.80% and an incident photon-to-current conversion efficiency of 84.6% providing a very promising candidate for sustainable energy production with a high performance/cost ratio.

KEYWORDS: self-standing TiO_2 nanotube arrays · anodized TiO_2 nanoparticles · layer-by-layer assembly · dye-sensitized solar cells · morphology

The soaring global energy demand and possible exhaustion of fossil fuels in the near future have driven the development of new types of renewable and sustainable alternatives. Of particular interests are the photovoltaic devices, which can directly and safely convert the solar light into electricity for widespread sustainable energy production. To rival the low-cost fossil-fuel-based electricity, solar energy must be utilized in a cost-effective fashion.[1] Compared with traditional silicon-based solar cells, the per-watt cost of dye-sensitized solar cells (DSCs) was significantly decreased, although lower power efficiency (η) was obtained.[2−4] The ordered TiO_2 nanotube arrays (TNAs) synthesized by the anodization method have been employed for DSCs due to the potential for the rapid unidirectional electron percolation since many particle boundaries were present in the disordered interstices of TiO_2 nanoparticles (TPs) interrupting transport of electrons.[5,6] Although novel structures of 3-dimensional DSCs,[7] bifacial DSCs,[8] shell/core DSCs,[9] layered TNA-TP DSCs,[10] and Ti-substrate flexible DSCs[11] have been recently developed based on TNAs, the back-illuminated geometries have inevitably resulted in a great energy loss by the light passage through the translucent electrolyte and counter electrode.[12] The front-illuminated DSCs could be fabricated by sputtering thin Ti film on a fluorine doped tin oxide (FTO) glass followed by anodization, but there was a limitation in increasing the thickness and area of TNAs and this procedure brought in additional production cost.[13] It is still a formidable challenge to improve the design of photoanodes with an elevated η and at the same time lower cost, since many hybrid structures do not possess high light harvesting efficiency, long photoelectron lifetime, desirable electron extraction, and facile operation simultaneously. To tackle these problems, here we combine the better light harvesting of front-illuminated geometries, unidirectional photoelectron transport through TNAs, and desirable electron extraction from hierarchical structures. The preparation, characterization, and photoelectric properties of hybrid morphologies and their application in DSCs are described in detail below.

RESULTS AND DISCUSSION

Invertible hierarchical structures of TNAs and TPs on FTO glasses are shown in Figure 1.

* Address correspondence to sbaik@me.skku.ac.kr.

Received for review March 29, 2011 and accepted May 17, 2011.

Published online May 20, 2011
10.1021/nn201169u

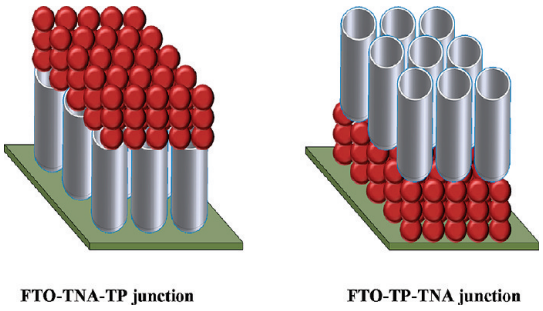

Figure 1. Schematic of layer-by-layer photoanode construction.

To fabricate these junctions, there are two prerequisites; (1) the brittle TNAs should keep their vertically aligned interconnected morphology during the annealing, film detachment, and transplanting process. (2) TPs should hold their place without clogging the open tops of TNAs to construct the FTO−TP−TNA junction.

The fabrication processes of layer-by-layer (LBL) hierarchical junctions are demonstrated in Figure 2. TNAs were self-assembled by electrochemical anodization in polar organic electrolyte, glycerol, containing a small amount of fluoride ions due to the dynamic equilibrium of top-to-bottom oxide formation and fluoride selective etching mechanism.[14,15] The two-step anodization was employed to produce highly ordered tube arrays with large aspect ratios.[16] The self-standing TNAs with an average inner diameter of 110 nm and a length of 9 μm were obtained by rinsing, annealing, and H_2O_2 etching of the anodized film (Figures 2a, b). A total number of 41 000 000 tubes were employed on the area of photoanodes (0.15 cm^2) as will be discussed shortly. TNAs could be employed as tube parts in the hierarchical structure or subsequently disintegrated by ultrasonication to produce TPs. This approach can provide low cost and great simplicity since both TNAs and TPs were produced by anodization rather than additionally employing other methods.

A postultrasonication treatment of TNAs in ethanol produced well-dispersed nanotubes in random orientation (Figure 2c). The tube length was decreased to 1−3 μm after ultrasonication at 150 W for 10 min. Further sonication at 280 W for 30 min could disintegrate nanotubes into TPs with a diameter of 20−35 nm which is in agreement with the crystallite size of TNAs.[17] Although a small number of residual nanotubes were observed at this condition (Figure 2d), prolonged sonication at stronger intensity would convert all the tubes into nanoparticles. The viscous paste was prepared by mixing TPs, terpinol, and ethyl cellulose. The paste was applied on the FTO glass by the doctor blade technique and annealed at 500 °C for 2 h to form a porous photoanode. Vigorous stirring and strong ultrasonication was used to prepare the

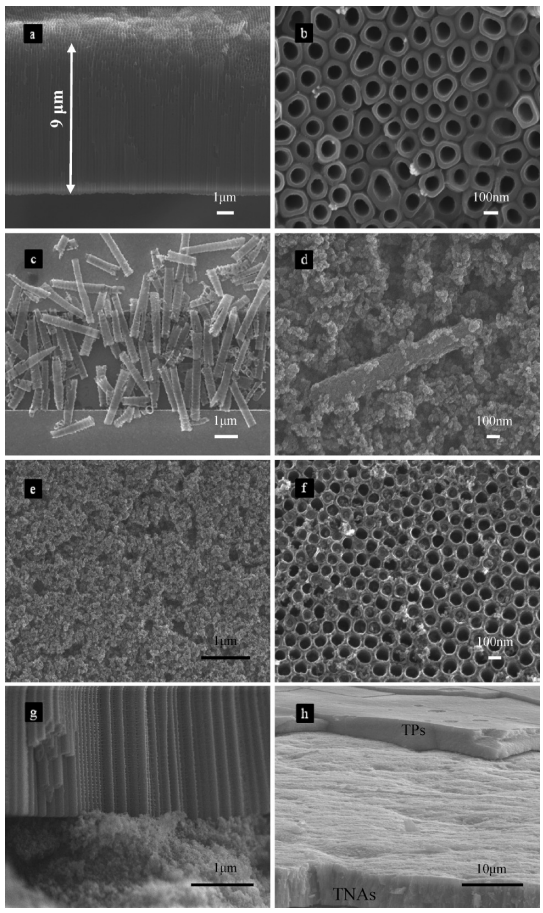

Figure 2. SEM images of the TNAs and TPs: (a) cross-sectional view of self-standing TNAs; (b) top view of TNAs; (c) randomly oriented TiO_2 nanotubes after sonication; (d,e) mesoporous TiO_2 nanoparticulate film at different magnifications; (f) top view of the FTO−TP−TNA junction; (g) side view of the FTO−TP−TNA junction; (h) side view of the FTO−TNA−TP junction. The TP layer on top of the TNA layer was partly removed for visualization.

homogeneous paste, and no serious aggregation of TPs was observed (Figure 2e). The self-standing TNAs were transplanted on top of the TP paste film to construct the FTO−TP−TNA junction (Figure 2f,g). Interestingly, some nanoparticles were found to position in the holes of nanotube arrays after annealing, which could be caused by the force of organic evaporation. However, the structure of interconnected network of vertically oriented nanotubular arrays was successfully protected and most of tubes were not clogged. The image of the FTO−TNA−TP junction is provided in Figure 2h.

After LBL assembly of TP films, the average thickness of layers 1, 2, and 3 (L) was 4, 8, and 11 μm, respectively, determined by a surface profilometer (Figure 3a). The X-ray diffraction (XRD) pattern of the TNAs on titanium substrate after the annealing process and before detachment is shown in Figure 3b. After annealing at 500 °C for 2 h, all TiO_2 tube structures were transformed into anatase, and Bragg Ti peaks could also be observed. The SnO_2 peaks were observed instead of Ti

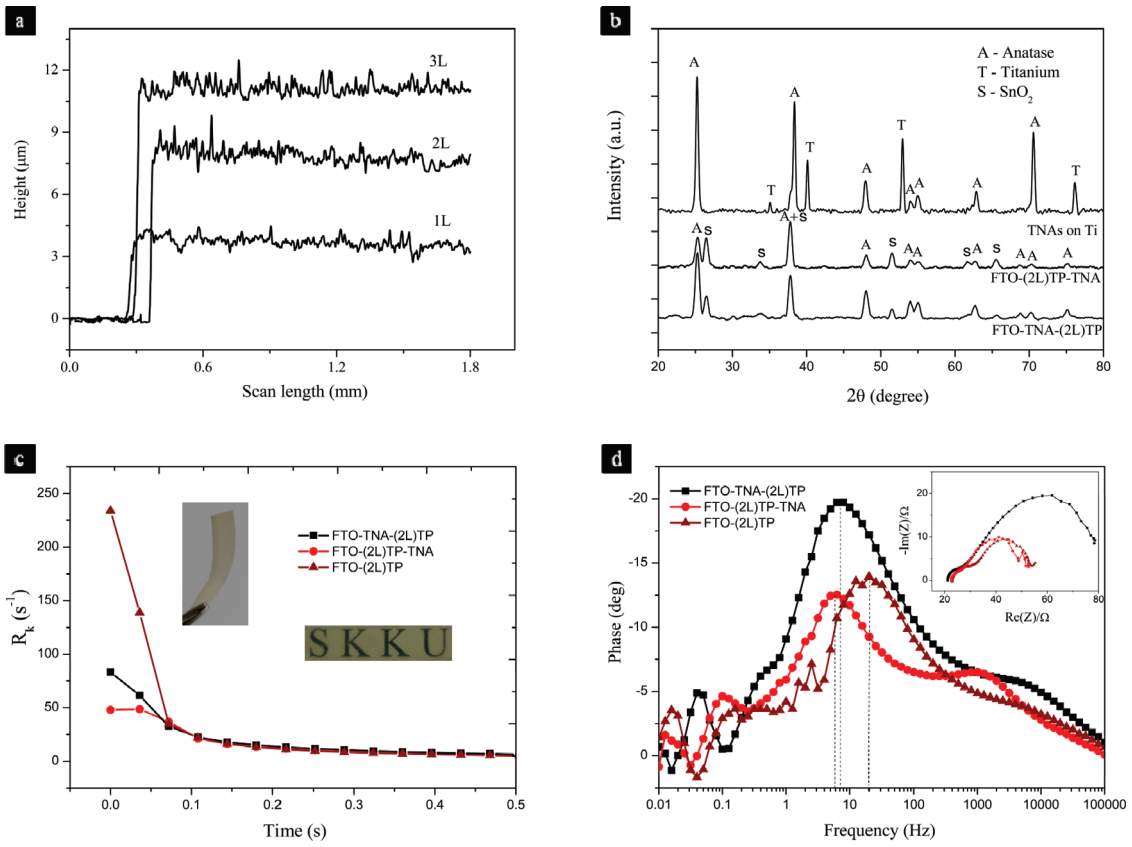

Figure 3. (a) Thickness of TP films (1−3 L) on FTO glass. (b) XRD patterns of the TNAs on Ti substrate (after annealing at 500 °C for 2 h) and hierarchical structures on FTO substrates. (c) Modified charge recombination rate. The transparency of the self-standing TNA film is demonstrated in inset images. (d) EIS data. Nyquist plot is shown in the inset.

peaks after the construction of LBL hierarchical junctions on FTO substrates. According to Scherrer's equation,[18] the calculated average diameter of TPs is 32 nm, which is in agreement with the SEM observation.

The open-circuit photovoltage, V_{oc}, during the dynamic relaxation from the standard global air mass (AM) 1.5 illuminated quasi-equilibrium state (E_{F_n}) to the dark equilibrium (E_{F_0}) can be derived by the following expression[19,20]

$$V_{oc} = \frac{E_{F_n} - E_{F_0}}{e} = \frac{K_B T}{e} \ln \frac{n}{n_0} \qquad (1)$$

where n is the free electron concentration in titania nanostructures, n_0 is the electron concentration in the dark equilibrium, K_B is the Boltzmann constant, T is the absolute temperature, and e is the positive elementary charge. Equation 1 indicates the free electron concentration is related with the open circuit voltage. The V_{oc} was initially at a steady state under the illumination at a constant intensity, and it gradually decreased to zero in the dark. The charge recombination rate $U(n)$ was defined as[20]

$$U(n) = -\frac{dn}{dt} \qquad (2)$$

The logarithmic change of the free electron concentration, which can be defined as a modified charge recombination rate R_k (s^{-1}), can be obtained using eq 3 by neglecting the change in T since n_0 is constant and n varies during the relaxation.

$$R_k = -\frac{d \ln(n)}{dt} = -\frac{e}{K_B T} \frac{dV_{oc}}{dt} \qquad (3)$$

Figure 3c shows transient R_K in the dark, and initial values of FTO−(2 L)TP, FTO−TNA−(2 L)TP and FTO−(2 L)TP−TNA junctions were 234.1, 83.2, and 47.9 s^{-1}, respectively. In comparison to the FTO−(2 L)TP photoanode, the incorporation of TNAs exhibited superior recombination characteristics. The free-standing TNA film was transparent, as shown in the inset images, extending the light passage. The letters which were placed below the TNA film could be clearly shown. The front-illuminated DSCs can increase the light harvesting efficiency by approximately 33% compared with back-illuminated DSCs.[21]

Figure 3d shows the Bode plot of electrochemical impedance spectroscopy (EIS) of three different junction structures measured with an alternating-current (AC) amplitude of 10 mV under the AM 1.5 illumination. The corresponding Nyquist plot is shown in the inset. In all the EIS Nyquist spectra, two well-defined semicircles were observed in the high frequency (>1 kHz) and medium frequency (1−100 Hz) regions. The high-frequency semicircle represents the redox reaction

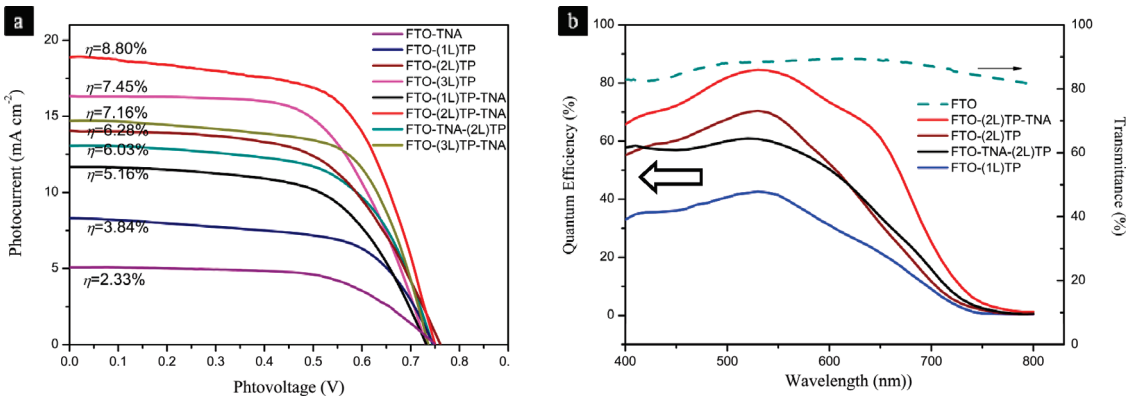

Figure 4. (a) *J*–*V* characteristics of DSCs fabricated using LBL assembly of TNAs and TPs; (b) IPCE characteristics of representative junction structures.

of I^-/I_3^- at the counter electrode, and the medium-frequency semicircle reflects the electron transfer at the FTO/TiO_2/dye/electrolyte interface.[22] The lifetime of photoelectrons (τ) in a photoanode can be calculated according to the equation $\tau = 1/\omega_{peak} = 1/(2_\pi f_{peak})$,[22] where ω_{peak} and f_{peak} are the peak angular frequency and oscillation frequency of the impedance semicircle at the medium frequency region. From the Bode plot, f_{peak} of FTO–(2 L)TP–TNA, FTO–TNA–(2 L)TP, and FTO–(2 L)TP junctions was 6, 8, and 20 Hz, respectively, and the corresponding τ was 27, 20, and 8 ms, respectively. The Nyquist plot revealed that the interfacial resistance FTO–TNA–(2 L)TP junction was significantly greater than those of other architectures leading to a lower η as will be discussed shortly.

Electron diffusion length L_n represents the average travel distance of electrons before recombining with acceptors.[23] It is related with the range of suitable thicknesses for semiconductor layers[24] and electron collection efficiency[25] in photovoltaic devices. L_n can be obtained by[26]

$$L_n = \sqrt{\tau D_n} = \sqrt{\tau \frac{d^2}{R_t C_u}} = d\sqrt{\frac{\tau}{R_t C_u}} \qquad (4)$$

where D_n is the electron diffusion coefficient, R_t and C_u are the equivalent resistance and capacitance of photoelectrodes, and d is the thickness of titania films. The calculated L_n of FTO–(2 L)TP–TNA, FTO–TNA–(2 L)TP, and FTO–(2 L)TP junctions is 42.97, 26.42, and 9.59 μm, respectively. The incorporation of self-standing TNAs with a high aspect ratio of ~80 into anodized TPs was favorable for electron diffusion through a longer distance with less grain boundaries. By fitting intensity modulated photocurrent spectroscopy (IMPS) and intensity modulated photovoltage spectroscopy (IMVS) data using a multiple trapping model,[27] the estimated electron diffusion length of TNAs was much longer than TPs, which is in agreement with our result.

Figure 4a shows the photocurrent density–voltage (*J*–*V*) characteristics of DSCs fabricated using various LBL structures of photoanodes under the AM 1.5 solar condition with an intensity of 100 mW cm^{-2}. The η of the TNA film (~9 μm thickness) on the FTO glass (FTO–TNA) was 2.33%. For the TP-coated FTO glasses, the increased layers of mesoporous TP films lead to an increase in η (from 3.84% of 1 L to 7.45% of 3 L). The construction of TNAs on top of TPs (FTO–TP–TNA junctions) was beneficial for the enhancement of η up to 2 L TPs. It was reported that the photoanode film thickness of 10 μm is optimal for TP based DSCs since nearly all of incident photons were absorbed.[28] The addition of TNAs on 3 L TPs with a thickness of 11 μm could hardly increase photon harvest and the unilluminated layer probably provided additional trapping sites for charge recombination. The η of FTO–(2 L)TP–TNA junction was 45.9% superior to its reverse structure of FTO–TNA–(2 L)TP suggesting the electron extraction from TPs to the FTO glass was better than that from TNAs to the FTO substrate due to the smaller interfacial resistance confirmed from the Nyquist spectra.

TABLE 1. The Photovoltaic Characterization Results of DSCs Based on Different Photoanodes

photoanode junctions	TiO_2 thickness (μm)	V_{oc} (V)	J_{sc} (mA cm^{-2})	ff (%)	η (%)
FTO–TNA	9	0.75	5.08	61.2	2.33
FTO–(1 L)TP	4	0.74	8.31	62.4	3.84
FTO–(2 L)TP	8	0.76	14.05	58.8	6.28
FTO–(3 L)TP	11	0.73	16.33	62.5	7.45
FTO–(1 L)TP–TNA	13	0.73	11.69	60.5	5.16
FTO–(2 L)TP–TNA	17	0.75	18.89	62.1	8.80
FTO–TNA–(2 L)TP	17	0.75	13.07	61.5	6.03
FTO–(3 L)TP–TNA	20	0.74	14.70	65.8	7.16

The photovoltaic characterization results are summarized in Table 1. To the best of our knowledge, maximum performances of the self-standing TNA-based DSC are a V_{oc} of 0.81 V, fill factor (ff) of 0.641, short-circuit photocurrent density (J_{sc}) of 15.46 mA cm^{-2} and η of 8.07%.[29] We achieved a V_{oc} of 0.75 V, ff of 0.621, J_{sc} of 18.89 mA cm^{-2} and η of 8.80% by the LBL assembly of self-standing TNAs and anodized TPs. This performance is quite remarkable

considering commercial Ru535-bisTBA was used without further purification.

Figure 4b shows transmittance of FTO glass and incident photon-to-current conversion efficiency (IPCE) spectra obtained from representative structures. The FTO−(2 L)TP−TNA junction shows an impressive response over a wide spectral range, even up to the long wavelength of 750 nm. This could be due to the enhanced photoelectron collection and light scattering through TNAs compared with the FTO−(2 L)TP junction. In the wavelength range between 420 and 630 nm, the peak IPCE value was as high as 84.6% resulting in the high J_{sc} of 18.89 mA cm^{-2} since J_{sc} can be approximately expressed by[6]

$$J_{sc} = q\eta_{lh}\eta_{inj}\eta_{cc}I_0 \quad (5)$$

Where q is the elementary charge; η_{lh} is the light-harvesting efficiency; η_{inj} is the charge-injection efficiency; η_{cc} is the IPCE; I_0 is the illuminated light intensity. Divided by the FTO transmittance, the internal quantum efficiency approached 90−97% in the wavelength region of 470−570 nm showing the effective functions of hierarchical construction in highly efficient DSCs.

CONCLUSION

A layer-by-layer hierarchical assembly of self-standing TiO_2 nanotube arrays onto TiO_2 nanoparticles extended the photoelectron lifetime by 237.5%. The better light harvesting of front-illuminated geometries, unidirectional electron transportation through nanotubes and desirable electron extraction from nanoparticles to the FTO layer resulted in a high performance of DSC (η = 8.80%, J_{sc} = 18.89 mA cm^{-2}, maximum IPCE = 84.6%). Both the TiO_2 nanotubes and TiO_2 nanoparticles were prepared by anodization providing a facile, cost-effective fabrication route. The efficiency would be further elevated by modulating the thickness of TNA and TP layer or improving the absorption property of sensitizing dyes.

METHODS

The Synthesis of TNAs and TPs. Potentiostatic anodization of Ti foils (99.99% purity, 0.25 mm thickness, Nilaco) was performed at 50 V in glycerol electrolyte containing 0.1 M NH_4F and 2 vol % deionized water using a platinum cathode.[30] After 1 h anodization, the developed TNA film was peeled off by sonication to produce a nanobowl array footprint. The second-step anodization was carried out under the same condition for 6 h to obtain highly ordered TNAs.[16] Before the termination of anodization, voltage was gradually decreased from 50 to 20 V within 20 s and then increased to 100 V immediately, holding constant for 5 s. The film was then washed by ethanol and deionized water and then annealed in a muffle furnace at 500 °C for 2 h. The annealed TNA/Ti foil was immersed in 33 wt % H_2O_2 solution for 5 min followed by rinsing and drying. The self-standing TNA film (~8 mm × 10 mm) could be separated from the Ti substrate by bending back and forth and peeling off using a razor blade. The TNA film was then cut by the razor blade into the size of 3 mm × 5 mm. TPs were obtained by sonicating TNAs at 280 W for 30 min in ethanol solution. The viscous TP paste was prepared by mixing TPs, terpinol, and ethyl cellulose at 20:70:10 wt %. Vigorous stirring and sonication was further used to ensure homogeneity and inhibit particle aggregation.

The Characterization of Hierarchical Junctions. The morphology was observed with a field-emission scanning electron microscope (JEOL, JEM2100F), and the crystal phase was characterized by an X-ray diffractiometer (Bruker, AXS-8 ADVANCE). The transmittance was investigated by a UV−vis spectrometer (Agilent, RSA-HP-8453) and the transient V_{oc} was recorded every 36 millisecond by a computer interfaced data logger (Agilent, 34970A). Film thickness was measured by a surface profilometer (KLA-Tencor, Alpha-Step IQ). EIS analysis was performed by a multichannel potentiostat/galvanostat (Biologic, VMP3).

The Fabrication of DSCs. For the preparation of the counter electrode, Pt was sputtered onto the clean FTO glass (8Ω/cm^2, NSG) at a constant current of 20 mA for 5 min (Cressington, 108auto) using Ar as a jet gas. For the photoanode preparation, the FTO glass was pretreated by 45 mM $TiCl_4$ solution at 70 °C for 30 min. To immobilize the self-standing TNA film onto the FTO substrate, a drop of glycerol was first applied onto the FTO glass. The TNA film was transferred onto glycerol using a tweezer. After the vacuumization at 120 °C (Neuronfit, DZF-6020) for 30 min, good adhesion between the TNA film and the FTO substrate could be obtained which could be further improved by $TiCl_4$ treatment and annealing. To construct the FTO−TP−TNA junction, the doctor blade technique was first employed to coat thin viscous TP film onto the FTO glass. The TP-coated FTO glass was placed on a hot plate and the temperature was increased to 150 °C. In the next step, the TNA film was gently placed on the viscous TP layer using a tweezer followed by annealing in a muffle furnace at 500 °C for 2 h. To construct the FTO−TNA−TP junction, TPs were coated onto the annealed TNA−FTO anode, and followed by solidification and further annealing. All the annealed TiO_2 photoanodes were repeatedly treated by $TiCl_4$ and annealing followed by irradiation under the simulated solar light for 20 min. The photoanodes were then immersed into 0.5 mM *cis*-di(thiocyanato)-bis(2,2′-biprydil-4.4′-dicarboxylato)ruthenium(II)-bis-tetrabutylammonium (Ru535-bisTBA, Solaronix) in 1:1 acetonitrile and *tert*-butanol for 24 h. The sandwich type cells were fabricated by assembling the photoanodes, counter electrodes, and electrolyte together. The electrolyte, containing 0.6 M 1,2-dimethyl-3-propyl imidazolium iodide, 0.5 M LiI, 0.05 M I_2, and 0.5 M 4-*tert*-butylpyridine in acetonitrile, was introduced into the cell cavity *via* a vacuum filling method. The hot melting plastic thin film (Dupont, Surlyn 1702) was used as a spacer to combine two electrodes with the cavity inside.

Solar Cell Characterization. *J*−*V* characteristics of DSCs were measured by a Keithley 2400 source meter under the AM 1.5 simulated sunlight (Oriel, Sol 3ATM). The active area of working electrodes was about 0.15 cm^2 with a relative error of ±5% determined by a computer calibrated optical microscope (Olympus, SZ61) equipped with a digital camera (Artray, 130MI-DS). A 5 mm × 3 mm illumination mask was also used to further define the testing area. The IPCE plots were obtained by Oriel IQE 200.

Acknowledgment. This work was supported by the Center for Nanoscale Mechatronics & Manufacturing (2009K000160) which is a 21st Century Frontier Research Program, the Basic Science Research Program (2011-0004463), and the WCU (World Class University) Program (R31-2008-10029) through the NRF Korea funded by the MEST.

REFERENCES AND NOTES

1. Lewis, N. S. Toward Cost-Effective Solar Energy Use. *Science* **2007**, *315*, 798–801.

2. Green, M. A.; Emery, K.; Hishikawa, Y.; Warta, W. Solar Cell Efficiency Tables (Version 37). *Prog. Photovolt. Res. Appl.* **2011**, *19*, 84–92.
3. O'Regan, B.; Grätzel, M. A Low-Cost, High-Efficiency Solar Cell Based on Dye-Sensitized Colloidal TiO_2 Films. *Nature* **1991**, *353*, 737–740.
4. Chen, C. Y.; Wang, M.; Li, J. Y.; Pootrakulchote, N.; Alibabaei, L.; Ngoc-Le, C. H.; Decoppet, J. D.; Tsai, J. H.; Grätzel, C.; Wu, C. G.; *et al*. Highly Efficient Light-Harvesting Ruthenium Sensitizer for Thin-Film Dye-Sensitized Solar Cells. *ACS Nano* **2009**, *3*, 3103–3109.
5. Liu, Z.; Zhang, X.; Nishimoto, S.; Jin, M.; Tryk, D. A.; Murakami, T.; Fujishima, A. Highly Ordered TiO_2 Nanotube Arrays with Controllable Length for Photoelectrocatalytic Degradation of Phenol. *J. Phys. Chem. C* **2008**, *112*, 253–259.
6. Zhu, K.; Neale, N. R.; Miedaner, A.; Frank, A. J. Enhanced Charge-Collection Efficiencies and Light Scattering in Dye-sensitized Solar Cells Using Oriented TiO_2 Nanotubes Arrays. *Nano Lett.* **2007**, *7*, 69–74.
7. Liu, Y.; Li, M.; Wang, H.; Zheng, J. M.; Xu, H. M.; Ye, Q. H.; Shen, H. Synthesis of TiO_2 Nanotube Arrays and Its Application in Mini-3D Dye-Sensitized Solar Cells. *J. Phys. D: Appl. Phys.* **2010**, *43*, 205103.
8. Liu, Z. Y.; Misra, M. Bifacial Dye-Sensitized Solar Cells Based on Vertically Oriented TiO_2 Nanotube Arrays. *Nanotechnology* **2010**, *21*, 125703.
9. Roy, P.; Kim, D.; Paramasivam, I.; Schmuki, P. Improved Efficiency of TiO_2 Nanotubes in Dye Sensitized Solar Cells by Decoration with TiO_2 Nanoparticles. *Electrochem. Commun.* **2009**, *11*, 1001–1004.
10. Yun, H. G.; Park, J. H.; Bae, B. S.; Kang, M. G. Dye-Sensitized Solar Cells with TiO_2 Nano-Particles on TiO_2 Nano-Tube-Grown Ti Substrates. *J. Mater. Chem.* **2011**, *21*, 3558–3561.
11. Kuang, D.; Brillet, J.; Chen, P.; Takata, M.; Uchida, S.; Miura, H.; Sumioka, K.; Zakeeruddin, S. M.; Grätzel, M. Application of Highly Ordered TiO_2 Nanotube Arrays in Flexible Dye-Sensitized Solar Cells. *ACS Nano* **2008**, *2*, 1113–1116.
12. Shankar, K.; Mor, G. K.; Prakasam, H. E.; Yoriya, S.; Paulose, M.; Varghese, O. K.; Grimes, C. A. Highly-ordered TiO_2 Nanotube Arrays up to 220 μm in Length: Use in Water Photoelectrolysis and Dye-Sensitized Solar Cells. *Nanotechnology* **2007**, *18*, 065707.
13. Mor, G. K.; Varghese, O. K.; Paulose, M.; Grimes, C. A. Transparent Highly Ordered TiO_2 Nanotube Arrays *via* Anodization of Titanium Thin Films. *Adv. Funct. Mater.* **2005**, *15*, 1291–1296.
14. Mor, G. K.; Varghese, O. K.; Paulose, M.; Mukherjee, N.; Grimes, C. A. Fabrication of Tapered, Conical-Shaped Titania Nanotubes. *J. Mater. Res.* **2003**, *18*, 2588–2593.
15. Xu, X.; Fang, X.; Zhai, T.; Zeng, H.; Liu, B.; Hu, X.; Bando, Y.; Golberg, D. Tube-in-Tube TiO_2 Nanotubes with Porous Walls: Fabrication, Formation Mechanism, and Photocatalytic Properties. *Small* **2011**, *7*, 445–449.
16. Wang, D.; Yu, B.; Wang, C.; Zhou, F.; Liu, W.; Novel, A Protocol Toward Perfect Alignment of Anodized TiO_2 Nanotubes. *Adv. Mater.* **2009**, *21*, 1964–1967.
17. Yu, J.; Dai, G.; Cheng, B. Effect of Crystallization Methods on Morphology and Photocatalytic Activity of Anodized TiO_2 Nanotube Array Films. *J. Phys. Chem. C* **2010**, *114*, 19378–19385.
18. Cademartiri, L.; Montanari, E.; Calestani, G.; Migliori, A.; Guagliardi, A.; Ozin, G. A. Size-Dependent Extinction Coefficients of PbS Quantum Dots. *J. Am. Chem. Soc.* **2006**, *128*, 10337–10346.
19. Bisquert, J.; Zaban, A.; Salvador, P. Analysis of the Mechanisms of Electron Recombination in Nanoporous TiO_2 Dye-Sensitized Solar Cells. Nonequilibrium Steady-State Statistics and Interfacial Electron Transfer *via* Surface States. *J. Phys. Chem. B* **2002**, *106*, 8774–8782.
20. Zaban, A.; Greenshtein, M.; Bisquert, J. Determination of the Electron Lifetime in Nanocrystalline Dye Solar Cells by Open-Circuit Voltage Decay Measurements. *ChemPhysChem* **2003**, *4*, 859–864.
21. Varghese, O. K.; Paulose, M.; Grimes, C. A. Long Vertically Aligned Titania Nanotubes on Transparent Conducting Oxide for Highly Efficient Solar Cells. *Nat. Nanotechnol.* **2009**, *4*, 592–597.
22. Kern, R.; Sastrawan, R.; Ferber, J.; Stangl, R.; Luther, J. Modeling and Interpretation of Electrical Impedance Spectra of Dye Solar Cells Operated under Open-Circuit Conditions. *Electrochim. Acta* **2002**, *47*, 4213–4225.
23. Gonzalez-Vazquez, J. P.; Anta, J. A.; Bisquert, J. Determination of the Electron Diffusion Length in Dye-Sensitized Solar Cells by Random Walk Simulation: Compensation Effects and Voltage Dependence. *J. Phys. Chem. C* **2010**, *114*, 8552–8558.
24. Bandić, Z. Z.; Bridger, P. M.; Piquette, E. C.; McGill, T. C. Electron Diffusion Length and Lifetime in P-Type GaN. *Appl. Phys. Lett.* **1998**, *73*, 3276–3278.
25. Wong, D. K. P.; Ku, C. H.; Chen, Y. R.; Chen, G. R.; Wu, J. J. Enhancing Electron Collection Efficiency and Effective Diffusion Length in Dye-Sensitized Solar Cells. *ChemPhysChem* **2009**, *10*, 2698–2702.
26. He, G.; Zhao, L.; Zheng, Z.; Lu, F. Determination of Electron Diffusion Coefficient and Lifetime in Dye-Sensitized Solar Cells by Electrochemical Impedance Spectroscopy at High Fermi Level Conditions. *J. Phys. Chem. C* **2008**, *112*, 18730–18733.
27. Jennings, J. R.; Ghicov, A.; Peter, L. M.; Schmuki, P.; Walker, A. B. Dye-Sensitized Solar Cells Based on Oriented TiO_2 Nanotube Arrays: Transport, Trapping, and Transfer of Electrons. *J. Am. Chem. Soc.* **2008**, *130*), 13364–13372.
28. Ito, S.; Takeuchi, T.; Katayama, T.; Sugiyama, M.; Matsuda, M.; Kitamura, T.; Wada, Y.; Yanagida, S. Conductive and Transparent Multilayer Films for Low-Temperature-Sintered Mesoporous TiO_2 Electrodes of Dye-Sensitized Solar Cells. *Chem. Mater.* **2003**, *15*, 2824–2828.
29. Lei, B. X.; Liao, J. Y.; Zhang, R.; Wang, J.; Su, C. Y.; Kuang, D. B. Ordered Crystalline TiO_2 Nanotube Arrays on Transparent FTO Glass for Efficient Dye-Sensitized Solar Cells. *J. Phys. Chem. C* **2010**, *114*, 15228–15233.
30. Macak, J. M.; Tsuchiya, H.; Taveira, L.; Aldabergerova, S.; Schmuki, P. Smooth Anodic TiO_2 Nanotubes. *Angew. Chem., Int. Ed.* **2005**, *44*, 7463–7465.